Environ Earth Sci (2015) 73:6035–6045
DOI 10.1007/s12665-015-4367-x

THEMATIC ISSUE

Extended finite element method for analysis of multi-scale flow in fractured shale gas reservoirs

Yongming Li[1] · Youshi Jiang[1] · Jinzhou Zhao[1] · Changyu Liu[1] · Liehui Zhang[1]

Received: 21 September 2014 / Accepted: 29 March 2015 / Published online: 10 April 2015

Abstract Economic exploration for shale gas is highly dependent on the complexity of the fracture network caused by hydraulic fracturing technology, so it is necessary to accurately assess the effect of the fracture network on gas flow behavior and productivity. Having multiple scales is a remarkable characteristic of gas flow in fractured shale gas reservoirs, which involves multiple flow regimes, including the gas desorption from shale matrix, Knudsen flow in nanoscale pores, Darcy flow in general porous media, Darcy flow in the fracture networks and fluid exchange between the matrix system and the fracture system. The extended finite element method (XFEM) has been integrated with the dual-permeability method (DPM) to investigate the multi-scale problem. Some previous studies have adopted the same solution scheme, but usually considered gas flow in the natural fracture network and in the hydraulic fractures as belonging to the same scale, and in addition, the coverage area of the stimulated reservoir volume (SRV) was underestimated. Based on the XFEM–DPM, this paper subsumes flow in the micro-mecro fractures and macro-hydraulic fractures under two scales because of their different effects on shale gas flow and then presents a new multi-scale extended finite element model to study the multi-scale flow problem in shale gas reservoirs. Moreover, the Lagrangian multiplier method is integrated to introduce the internal well boundary conditions into the XFEM, so the arbitrariness and the asymmetry of the complex fracture network can be taken into account easily to reflect the real flow mechanisms in fractured shale. Case studies indicate that the improved extended finite element model constructed in this paper is effective, especially for complicated asymmetrical physical condition problems.

Keywords Shale gas · Complex fracture network · Multi-scale flow · Extended finite element method · Lagrangian multiplier method · Multiple scale fractures

Abbreviations

H_f	Reservoir thickness (m)
β_ρ	Gas compressibility (Pa^{-1})
B_g	Gas volume factor (m^3/m^3)
k	Permeability in the x/y direction (m^{-2})
K	Permeability tensor (m^2)
μ	Gas viscosity (Pa·s)
t	Time (s)
w_d	Fracture width along the direction parallel to the fracture line (m)
λ	Lagrangian multiplier
ρ	Gas density (kg/m^3)
φ	Porosity
M_g	Molecular weight of methane (kg/mol)
τ_h	Tortuosity
b	Slip coefficient
ρ_s	Material density of shale sample (kg/m^3)
p_{wf}	Flowing bottomhole pressure (Pa)
p	Pressure (Pa)
Z	Real gas compressibility factor
C_t	Total gas compressibility
$\bar{q}_w$	Mass flow rate on the Dirichlet boundary condition (kg/s)
r	Distance between any point on the hydraulic fracture line and its corresponding wellbore

✉ Youshi Jiang
jiangyswpu@gmail.com

[1] State Key Laboratory of Oil and Gas Reservoir Geology and Exploitation, Southwest Petroleum University, Chengdu 610500, China

r_w Radius of wellbore (m)
n_f Number of fractures
q_L Langmuir gas volume (std m^3/kg)
p_L Langmuir gas pressure (MPa)
α Matrix–fracture transfer shape factor
Q^{ext} External flux vector

Subscript

x, y Space coordinates in global Cartesian coordinates
x', y' Space coordinates in local Cartesian coordinates
m Matrix
f Micro-mecro scale fracture
F Macroscale fracture

Superscript

enr Enrichment term
int Interfacial flux vector
ext External flux vector
T Transpose of matrix

Introduction

Economic exploration for shale gas is highly dependent on the complexity of the fracture network caused by hydraulic fracturing technology as well as the coverage area. It is very important to accurately assess the effect of the fracture network on gas flow feature and productivity. However, due to the multiple flow regimes and the strong multi-scale behavior, modeling for multi-scale flow in the fractured shale reservoir is challenging but worthwhile, and many researchers have done some meaningful work on this issue.

Having multiple scales is a characteristic of the flows in a fractured shale reservoir which involves multiple mechanisms, including gas desorption from matrix, Knudson flow in nanoscale pores, Darcy flow in the porous media, Darcy flow in the fracture networks and fluid exchange between the matrix system and the fracture system. Researchers proposed a lot of models with the multi-scale problem to tackle based on various methods including the analytical method (Ozkan et al. 2011; Brown et al. 2011), the semi-analytical method (Medeiros 2007a; Medeiros et al. 2007b) and the numerical method (Dershowitz et al. 2000; Cipolla et al. 2010; Kristinof et al. 2010; Sheng et al. 2012).

Ozkan et al. (2011) and Brown et al. (2011) adopted the trilinear analytical model to couple the flow in three environments: a tight, homogeneous reservoir beyond the tips of the hydraulic fractures (outer reservoir), a naturally fractured reservoir between hydraulic fractures (inner reservoir) and hydraulic fractures distributed along the length of the horizontal well. Their studies highlighted the effect of the SRV consisting of the hydraulic and natural fractures and noted that the production beyond the stimulated reservoir volume can be negligible (Carratú 2013).

Medeiros (2007a) proposed a semi-analytical model to investigate the performances of horizontal wells with multiple fractures. They solved the diffusivity equation on the basis of Green's function solution and utilized dual-porosity idealization to cope with the flow in the SRV. Medeiros et al. (2007b) further obtained several important conclusions in which the most important one is that the variation of stress distribution caused by hydraulic fracturing may significantly promote the formation of the fracture networks and the productivity. Based on the finite difference method, Cipolla et al. (2010) studied the impact of the conductivity of the hydraulic fractures on productivity. Cherubini et al. (2013) carried out a 3D finite element simulation to analyze the impact of single inclined faults on the fluid flow. Huang et al. (2014) coupled the discrete fracture model and the continuum model to simulate groundwater flow in fractured rocks, based on domain decomposition.

The XFEM was initially proposed to tackle the strong-discontinuity problem in relation to crack growth and was soon extended to other problems characterized by localization, complex geometries and multi-phase. The method has two main advantages over other numerical methods. The first is that the modeling of arbitrary geometric features can be independent of the mesh. The second is that the local field can be accurately reproduced based on the theory of partition of unity (Melenk and Babuška 1996). Belytschko and Black (1999) first presented the essential ideas of modeling crack growth by finite elements with minimal remeshing and adopting a discontinuous function to enrich the approximation. Moës et al. (1999) further improved Belytschko and Black's work by introducing the Heaviside function and the near-tip asymptotic function to capture the strong-discontinuity behavior. Many researchers developed the XFEM to solve problems for weak discontinuity such as interface problems and fluid flow in fractured reservoir. Sukumar et al. (2001) combined the level set method with the XFEM to represent the weak discontinuity due to material interfaces in composite. Réthoré et al. (2007, 2008) adopted a two-scale approach to model fluid flow in fractured porous media, and at the fine scale, the flow in the fracture was modeled using Stokes equations. Mohammadnejad and Khoei (2013a, b) regarded the pressure gradient jump across the hydraulic fracture as the weak discontinuity and established a fully coupled extended finite element model for modeling hydraulic fracture propagation.

Lamb et al. (2010) first combined the DPM and the XFEM to analyze coupled deformation and fluid flow in fractured porous media and demonstrated the validity of

the weak-discontinuity enrichment scheme. On the basis of Lamb's work, Sheng et al. (2012) built an XFEM–DPM model for multi-scale flow in fractured shale gas reservoir which integrated multiple flow regimes including mass transfer between matrix and fractures, four kinds of flow regimes and pressure dependence. Both Lamb's work and Sheng's work are meaningful, but have some shortcomings. Firstly, all the fractures are treated as micro-mecro scale fractures, including the macroscale hydraulic fractures which dominate the main flow direction. Secondly, the domain of dual-permeability media is unreasonably confined in the small finite elements which are bisected by the fractures, so the coverage area of the fracture network characterized by the SRV is underestimated and should be enlarged. Thirdly, they usually located the wellbore on the outer boundary of the whole domain rather than its interior according to the assumption of symmetry which did not always make sense, because both the complex fracture network and the reservoir were usually asymmetrical.

This paper aims to improve Lamb's and Sheng's work. The complex fracture network is further subsumed under two scales (the micro-mecro scale fracture network and the macroscale hydraulic fractures) according to their different impact on gas flow, and the flow in the two scales of fractures is strongly coupled. The notion of SRV is highlighted to reflect the coverage area of the micro-mecro scale fracture network and its impact on draining shale gas. The dual-permeability method (DPM) is adopted to capture the flow behavior resulting from the micro-mecro scale fracture network in the SRV, and in the meantime, extended finite element method (XFEM) is used to tackle the strong-/weak-discontinuity problems in relation to the flow field variations of the fracture system and the matrix system across the macroscale fractures which dominate the main flow direction. Combined with the method of introducing the interior well boundary condition into the XFEM based on the theory of Lagrangian multiplier (Cheng 1999), the arbitrariness and the asymmetry of the model can be taken into account easily to represent the real flow behavior. This study improves the XFEM–DPM model for multi-scale flow in fractured shale gas reservoir and the corresponding solution scheme.

Governing equations

Descriptions of physical model

The whole domain Ω is divided into three adjacent parts, including matrix domain Ω_m (outer reservoir), SRV domain Ω_s (inner reservoir) and macroscale fracture domain Ω_F

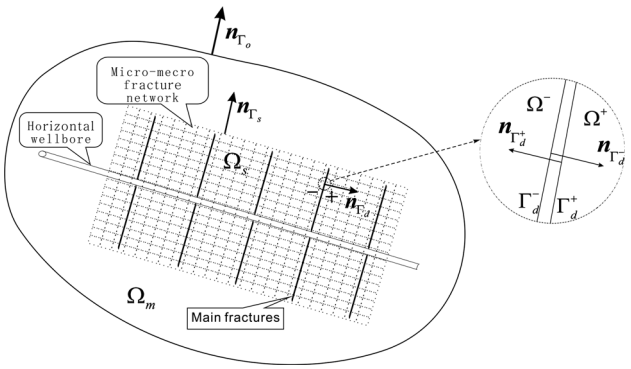

Fig. 1 Fluid flow in a hydraulically multi-fractured reservoir

(see Fig. 1). Ω is bounded by the outer boundary Γ_o, while Ω_s bounded by the exterior boundary Γ_s of the SRV and the interior boundary $\Gamma_d^+ \cup \Gamma_d^-$ which on the other side is the outer boundary of Ω_F. A fractured horizontal well with several hydraulic fractures is located in the domain. The macroscale hydraulic fractures dominate the main flow direction in the reservoir, and due to their high permeability and conductivity, they are defined and dealt with explicitly. The SRV domain is regarded as the dual-permeability media which involves numerous micro-mecro scale fractures. Every flow regime in the model is an isothermal event and obeys Darcy's law. The internal boundary conditions related to the wellbore include the Dirichlet boundary condition on Γ_w and the Neumann boundary condition on Γ_ϕ.

$\boldsymbol{n}_{\Gamma_o}$ and $\boldsymbol{n}_{\Gamma_s}$ are the unit outward normal to Ω and Ω_s, respectively. $\boldsymbol{n}_{\Gamma_d}$ is the unit normal vector to the discontinuity pointing to Ω^+ ($\boldsymbol{n}_{\Gamma_d} = \boldsymbol{n}_{\Gamma_d^-} = -\boldsymbol{n}_{\Gamma_d^+}$).

Fluid flow in multi-fractured shale involves multiple scale flow regimes, including the gas desorption from the shale matrix, Knudsen flow in nanoscale pores, Darcy flow in the micro-mecro scale fracture network and Darcy flow in the macroscale hydraulic fractures. The last two kinds of flow regimes are coupled by considering mass transfer between the two scale fractures.

The impermeable boundary conditions are imposed on the external and the internal boundary of the matrix system as

$$\frac{\partial p_m}{\partial \boldsymbol{n}} = 0 \quad \text{on } \Gamma_o \cup \Gamma_d^+ \cup \Gamma_d^-, \tag{1}$$

The impermeable boundary conditions are also imposed on the external boundary of the SRV domain as

$$\frac{\partial p_f}{\partial \boldsymbol{n}} = 0 \quad \text{on } \Gamma_s. \tag{2}$$

In addition, mass transfer is considered to couple the fluid flow in the micro-mecro scale fracture network and the

macroscale fractures. The complementary coupling condition is written as

$$[[\dot{W}_f]]\boldsymbol{n}_{\Gamma_d} = [[\dot{W}_F]]\boldsymbol{n}_{\Gamma_d} = q_{wd} \quad \text{on } \Gamma_d \tag{3}$$

$[\![*]\!] = *^+ - *^-$ represents the difference between the corresponding values at the two fracture faces.The Dirichlet boundary condition and the Neumann boundary condition can be imposed on the wellbore according to different production modes as

$$p_f = p_{wf} \text{ on } \quad \Gamma_\phi. \tag{4}$$

$$\rho_F \frac{k_{x'F}}{\mu_F}\frac{\partial p_f}{\partial x'}\bigg|_w = \bar{q}_w \quad \text{on } \Gamma_w. \tag{5}$$

Improvements and assumptions

Lamb et al. (2010) first combined the DPM and the XFEM to model the fluid flow in fractured porous media, and further Sheng et al. (2012) adopted the same approach to study multi-scale flow problem in a fractured shale reservoir. Their works are very meaningful, but should still be improved. In this paper, mistakes that exist in several equations given by Sheng have been corrected and some improvements have been made in several aspects as follows:

(a) It is assumed that two scale fractures exist in hydraulically fractured shale. This kind of classification scheme is similar to the scheme proposed by Lee et al. (2000). The first scale refers to the numerous micro-mecro scale fractures which usually compose a network, while the second scale fractures are the hydraulic fractures in control of the main flow direction.

(b) Many research findings revealed that economic exploration for shale gas is highly dependent on the complexity and the coverage area of the fracture network which can be characterized by the SRV. In comparison with the previous works, this paper enlarges the coverage area of SRV of the model in accordance with the popular opinion, rather than confining SRV in the elements which are bisected by the fractures. In this study, the DPM is adopted to capture the behavior of flow in the micro-mecro scale fracture network in the SRV (namely "inner reservoir" defined by Ozkan et al. 2011). On the other hand, the XFEM is used to tackle the weak-discontinuity problems involving the matrix system and the fracture system.

(c) In the fractured shale reservoir, gas flows mainly from the porous matrix into the micro-mecro scale fracture network first, then into the macro-fractures and finally into the wellbore. In addition, the fracture pressure which falls quite faster and is weak discontinuous strongly affects the matrix pressure near the macro-fracture. So the direct fluid transfer between the matrix and the macro-fractures can be ignored, and both the matrix pressure field and the fracture pressure field are assumed to be weak discontinuous across the macroscale fractures.

(d) The model is constructed on the basis of real gas, instead of ideal gas.

(e) The fluid pressure within the fracture is assumed to be constant along the inward direction that is perpendicular to the fracture line, while the pressure gradient and the fluid flow are discontinuous.

Based on the above five main improvements, this paper uses the same mesh to approximate the fluid pressure in both the fracture and matrix systems.

Strong form

The flow in a hydraulically fractured shale reservoir involves two highly coupled systems, i.e., the multiple scale matrix and fracture systems.

The gas flow in the matrix is at nano-, micro- and macroscales due to the difference in pore diameter, molecular collisions and so on, while fractures can be classified into two scales (macro- and micro-mecro scales) according to their lengths and conductivities. Macroscale fractures denote the main fractures which can dominate the main flow direction. Micro-mecro scale fractures are numerous and usually compose fracture networks. First to be constituted are the strong-form equations corresponding to the matrix and the fracture systems.

The continuity equation for the porous flow in the shale matrix is written as

$$\begin{aligned}&\left[\rho_m\varphi_m C_{tm} + (1-\varphi_m)C_a\rho_m\beta_\rho - q_L\varphi_m\beta_{\phi m}\right]\frac{\partial p_m}{\partial t}\\ &-\nabla\left(\rho_m\frac{K_m}{\mu_m}\nabla p_m\right) + \alpha\frac{\rho_m K_m}{\mu_m}(p_m - p_f) = 0.\end{aligned} \tag{6}$$

Where C_a represents the nanoscale behavior and the impact of gas desorption from the bulk matrix on the flow in the shale matrix and is defined by Civan et al. (2011) as

$$C_a = \frac{\rho_s M_g}{\rho\beta_\rho V_{std}}\frac{q_L p_L}{(p_L + p)^2}. \tag{7}$$

C_{tm} denotes the total compressibility of shale gas. For the detailed derivation process of the differential Eq. (6), readers can refer to the papers published by Sheng et al. (2012) and Civan et al. (2011).

The continuity equation for the flow in the micro-mecro scale fracture network is written as

$$\rho_f \varphi_f C_{tf} \frac{\partial p_f}{\partial t} - \nabla\left(\rho_f \frac{K_f}{\mu_f}\nabla p_f\right) - \alpha \frac{\rho_m K_m}{\mu_m}(p_m - p_f) = 0 \tag{8}$$

In the DPM, the flow in the micro-mecro scale fracture network is seen as continuous field in most of the SRV domain, which is, however, weak discontinuous across the large-scale fracture due to the pressure gradient jump. The shape factor α is introduced to accurately describe the single-phase quasi-steady-state transfer flow between matrix and fracture (Warren and Root 1963; Lemonnier and Bourbiaux 2010).

The continuity equation for the flow in the macroscale fracture (main fracture) is written as

$$\rho_F \varphi_F C_{tF} \frac{\partial p_f}{\partial t} - \nabla'\left(\rho_F \frac{K_F}{\mu_F}\nabla' p_f\right) = 0, \tag{9}$$

$$\rho_F \varphi_F C_{tF} \frac{\partial p_f}{\partial t} - \nabla''\left(r\frac{\rho_F K_F}{\mu_F}\nabla'' p_f\right) = 0. \tag{10}$$

Equation 9 is used to describe the linear flow in the away-from-wellbore region of the macro-fracture, while Eq. 10 describes the radial flow in the near-wellbore region. The symbol ∇ denotes the vector gradient operator in the total Cartesian coordinate system (x, y), while ∇' denotes that in the local Cartesian coordinate system (x', y') (see Fig. 2). To account for the feature of radial flow in the near-wellbore egion of the main hydraulic fractures, we use another local Cartesian coordinate (r, y') and ∇'', respectively, to replace (x', y') and ∇'.

Weak form

According to the above strong-form equations, weak-form equations can be derived based on the Galerkin formulation. The two weak-form equations of flow in the micro-mecro scale fracture network and macroscale fracture can be coupled to get the governing equation of the fracture system by considering the fluid transfer.The weak form of the continuity equation of fluid flow in the shale matrix is given by

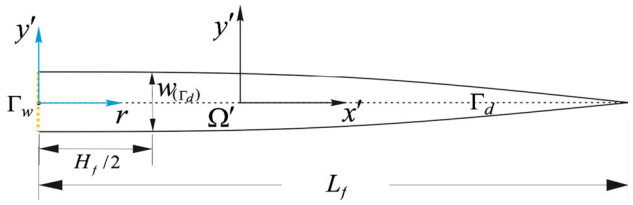

Fig. 2 Local Cartesian coordinate systems in the fracture

$$\begin{aligned}
&\int_\Omega \delta p_m \left[\rho_m \varphi_m C_{tm} + (1-\varphi_m)C_a \rho_m \beta_\rho - q_L \varphi_m \beta_\phi\right]\frac{\partial p_m}{\partial t} d\Omega \\
&+ \int_\Omega \nabla \delta p_m \cdot \rho_m \frac{K_m}{\mu_m}\cdot \nabla p_m d\Omega \\
&+ \int_\Omega \delta p_m \cdot \alpha \frac{\rho_m K_m}{\mu_m}\cdot (p_m - p_f) d\Omega = 0
\end{aligned} \tag{11}$$

Equation (11) is derived by the application of Galerkin–FEM, the divergence theorem and the boundary condition (Eq. 1) based on the strong form (Eq. 6).

In the reservoir domain outside the SRV, the third term on the left-hand side of Eq. 11 should be ignored.

The weak form of the continuity equation of fluid flow in the micro-mecro scale fracture network is therefore given by

$$\begin{aligned}
&\int_{\Omega_s} \delta p_f \left(\rho_f \varphi_f C_{tf}\right)\frac{\partial p_f}{\partial t} d\Omega + \int_{\Omega_s} \nabla \delta p_f \cdot \rho_f \frac{K_f}{\mu_f}\cdot \nabla p_f d\Omega_s \\
&+ \int_{\Gamma_d} \delta p_f \cdot \left[\!\left[\dot{W}_f\right]\!\right] \boldsymbol{n}_{\Gamma_d} d\Gamma \\
&- \int_{\Omega_s} \delta p_f \cdot \alpha \frac{\rho_m K_m}{\mu_m}\cdot (p_m - p_f) d\Omega_s = 0.
\end{aligned} \tag{12}$$

Similarly, the strong-form Eq. (8) is used to construct the Galerkin formulation, and the Divergence theorem and the inner boundary condition (Eq. 3) are adopted. In addition, the impermeable boundary condition (Eq. 13) is imposed on the external boundary of the SRV.

$$\int_{\Gamma_s} \delta p_f \cdot \rho_f \frac{K_f}{\mu_f}\cdot \nabla p_f \boldsymbol{n}_{\Gamma_s} d\Gamma_s = 0 \tag{13}$$

The weak form of the continuity equation of fluid flow in the macroscale fractures (main hydraulic fractures) is given by

$$\begin{aligned}
&\int_{\Gamma_d} \delta p_f \left(w_d \rho_F \varphi_F C_{tF}\right)\frac{\partial p_f}{\partial t} d\Gamma \\
&+ \int_{\Gamma_d} \frac{w_d \rho_F k_{x'F}}{\mu_F}\cdot \frac{\partial \delta p_f}{\partial x'}\cdot R(r)\cdot \frac{\partial p_f}{\partial x'} d\Gamma \\
&+ \int_{\Gamma_w} \delta p_f \cdot R(r)\cdot \bar{q}_w d\Gamma \\
&+ \int_{\Gamma_\phi} \left(\frac{\rho_F k_{x'F}}{\mu_F}\right)\cdot R(r)\cdot \left(\delta p_f \frac{\partial p_f}{\partial x'} + \frac{\partial \delta p_f}{\partial x'} p_f\right) d\Gamma \\
&- \int_{\Gamma_d} \delta p_f \left[\!\left[\dot{W}_F\right]\!\right] \boldsymbol{n}_{\Gamma_d} d\Gamma \\
&= \int_{\Gamma_\phi} \left(\frac{\rho_F k_{x'F}}{\mu_F}\right)\cdot R(r)\cdot \frac{\partial \delta p_f}{\partial x'} p_{wf} d\Gamma,
\end{aligned} \tag{14}$$

where

$$R(r) = \begin{cases} 1 & r > H_f/2 \\ r + r_w & 0 \le r \le H_f/2 \end{cases}. \tag{15}$$

r denotes the distance between any point on the hydraulic fracture line and its corresponding wellbore. The function $R(r)$ is defined to distinguish the radial flow in the near-wellbore region of the hydraulic fracture from the linear flow in the away-from-wellbore region of the hydraulic fracture. Fracture radial flow exists within a circle in the vertical plane with center at the wellbore and diameter equal to reservoir thickness H_f (Furui et al. 2003; Guo et al. 2009).

The Galerkin formulation of the strong-form Eq. 10 is given by

$$\int_{\Omega'} \delta p_f \left\{ \rho_F \varphi_F C_{tF} \frac{\partial p_f}{\partial t} - \nabla'' \left(r \frac{\rho_F K_F}{\mu_F} \nabla'' p_f \right) \right\} d\Omega' + \int_{\Gamma_\phi} \delta \lambda^{\mathrm{T}} (p_f - p_{wf}) \mathrm{d}\Gamma_\phi + \int_{\Gamma_\phi} \lambda^{\mathrm{T}} \delta (p_f - p_{wf}) \mathrm{d}\Gamma_\phi = 0 \tag{16}$$

The second row of Eq. (16) is introduced to load the Dirichlet boundary condition on the internal boundary of the reservoir according to the method of the Lagrangian multiplier.

Equation 16 can be solved by the application of the Divergence theorem and the assumption (e) which can lead to simplification, as indicated by Eq. 17.

$$\int_{\Omega'} \nabla' \delta p_f \frac{\rho_F K_F}{\mu_F} \nabla' p_f d\Omega' = \int_{\Gamma_d} \frac{\partial \delta p_f}{\partial x'} \frac{w_d \rho_F k_{x'F}}{\mu_F} \frac{\partial p_f}{\partial x'} d\Gamma. \tag{17}$$

Assuming that at any point on the macroscale fracture lines, the pressures of the two-scale fracture media are the same, couple the flow in the micro-mecro scale fracture network and the macro-fractures by canceling the fluid transfer terms in Eqs. 12 and 14, and finally the coupled governing equation of gas flow in the fracture system can be derived.

Calculation formula of productivity

The total productivity of multi-fractured horizontal well can be predicted by adding together the productivity of all the hydraulic fractures.

$$Q = \sum_{i=1}^{2n_F} \frac{\pi r_w k_F w_F}{\mu B_g} \frac{\partial p_F}{\partial r}\bigg|_{(r=r_w)_i} \tag{18}$$

Skin factor S can be easily taken into account by substituting the effective wellbore radius for the actual wellbore radius r_w or adopting the equivalent permeability in the near-wellbore region of hydraulic fracture.

Table 1 Reported reservoir and well data

Name of parameters (unit)	Value
Reservoir thickness (m)	50
Length in the x direction (m)	240
Length in the y direction (m)	240
Matrix intrinsic permeability (D)	5.3×10^{-7}
Matrix porosity	0.05
Micro-mecro fracture intrinsic permeability (D)	2×10^{-3}
Micro-mecro fracture porosity	4×10^{-3}
Macro-fracture intrinsic permeability (D)	Infinite
Macro-Fracture porosity	0.3
Wellbore radius (m)	0.068
Skin factor	0
Half fracture lengths (m)	60
Fracture width (m)	0.005
Distance between main fractures (m)	100
Shape factor	10
Initial pressure (MPa)	21.4
Bottomhole flowing pressure	6.9
Temperature in the reservoir (K)	333.33
Langmuir gas volume (std m^3/kg)	0.01
Langmuir gas pressure (MPa)	7.5

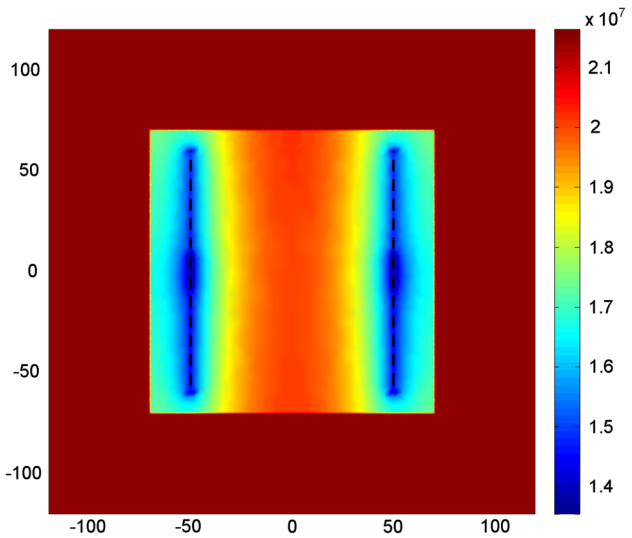

Fig. 3 Matrix pressure distribution (0.1 day)

Discretization formulation

The extended finite element method

According to assumption (c), both the matrix pressure field and the fracture pressure field are assumed to be weak

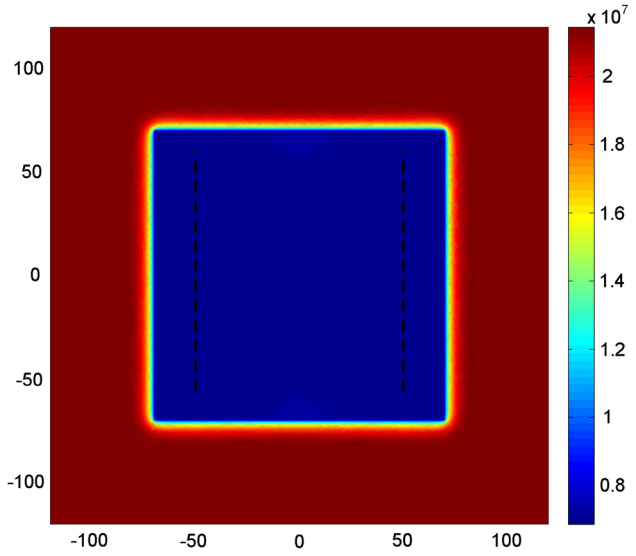

Fig. 4 Matrix pressure distribution (10 days)

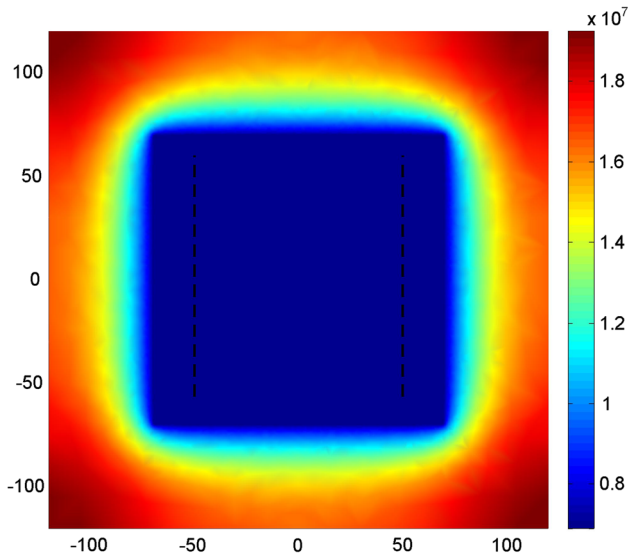

Fig. 5 Matrix pressure distribution (1000 days)

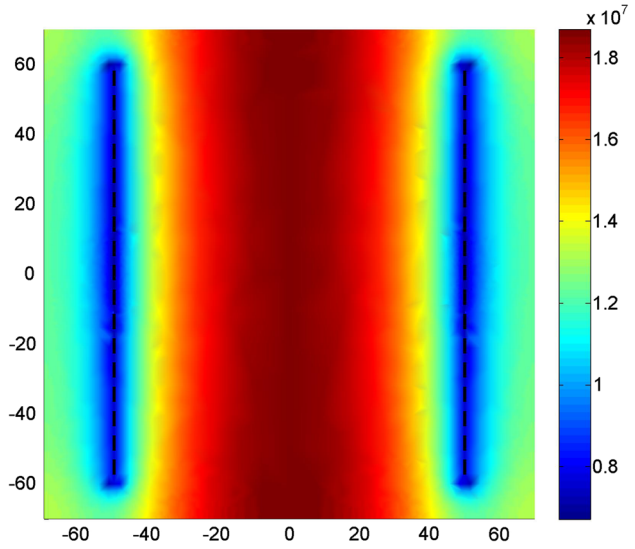

Fig. 6 Fracture pressure distribution (0.1 day)

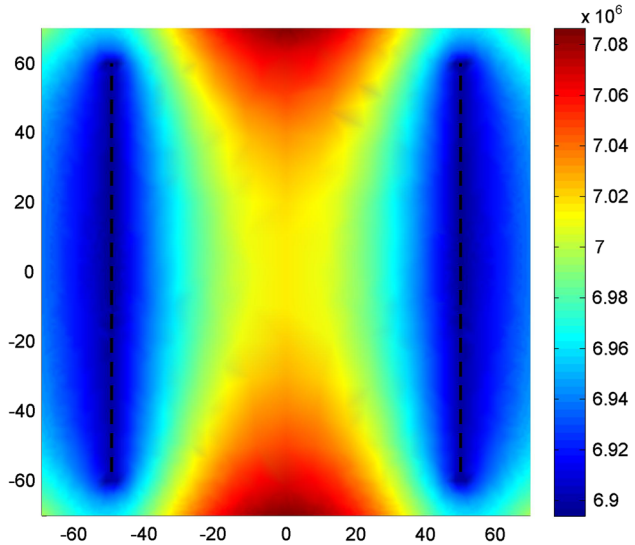

Fig. 7 Fracture pressure distribution (10 days)

discontinuous across the main fracture line. The fluid flow jump across the main fracture line can be reflected by using the improved weak-discontinuity enrichment function given by Moës et al. (2003).

The fracture pressure is approximated as the linear combination of the standard and enriched shape function as

$$p^h(\boldsymbol{x}) = \sum_{i \in N} N_i(\boldsymbol{x}) P_i + \sum_{j \in N_s^{enr}} N_j(\boldsymbol{x}) \left[\Phi(\boldsymbol{x}) - \Phi(\boldsymbol{x}_j) \right] a_j, \quad (19)$$

where $N_i(\boldsymbol{x})$ is the classical finite element shape function; P_i is the nodal value; and a_j is the additional degree of freedom at the enriched nodes. I is a set of all nodes, while J is a set of all enriched nodes. Nodes in J are such that their support are bisected by a single fracture. The first term on the right-hand side of Eq. 19 represents the classical finite element approximation, while the second term denotes the weak-discontinuous enrichment.

In the second term, the improved enrichment function is utilized to avoid a decrease in the convergence rate of the blending element. The shape enrichment function and its gradient are given by

$$\Phi(\boldsymbol{x}) = \sum_I |\phi(\boldsymbol{x}_I)| N_I(\boldsymbol{x}) - \left| \sum_I \phi(\boldsymbol{x}_I) N_I(\boldsymbol{x}) \right|, \quad (20)$$

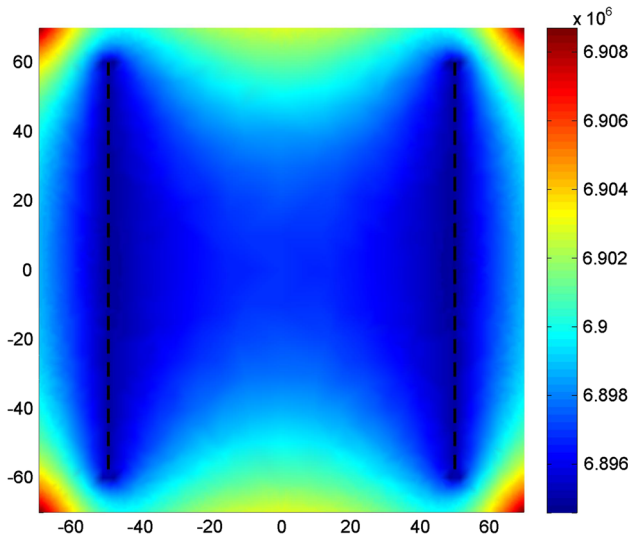

Fig. 8 Fracture pressure distribution (1000 days)

$$\nabla\Phi(\boldsymbol{x})\cdot\boldsymbol{n}_{\Gamma_d}=\sum_I|\phi(\boldsymbol{x}_I)|\nabla N_I(\boldsymbol{x})\boldsymbol{n}_{\Gamma_d}+H(\phi(\boldsymbol{x}))\cdot\sum_I\phi(\boldsymbol{x}_I)\nabla N_I(\boldsymbol{x})\boldsymbol{n}_{\Gamma_d},\tag{21}$$

The general Heaviside function $H(\phi(\boldsymbol{x}))$ (Eq. 22) makes the gradient of the enrichment function discontinuous across the fracture line, while the enrichment function itself is continuous.

$$H(\boldsymbol{x})=\begin{cases}1 & if \quad (\boldsymbol{x}-\boldsymbol{x}^*)\cdot\boldsymbol{n}_{\Gamma_d}>0\\ -1 & else\end{cases}.\tag{22}$$

Discretized form of the governing equations

Based on the extended finite element method, the discretized form of the governing Eqs. (11), (12) and (14) is as follows:

$$\boldsymbol{Q}_{mm}\dot{\boldsymbol{P}}_m+\boldsymbol{C}_{mm}\boldsymbol{P}_m+\boldsymbol{T}_{mm}\boldsymbol{P}_m-\boldsymbol{T}_{mf}\boldsymbol{P}_f=0,\tag{23}$$

$$\boldsymbol{Q}_{ff}\dot{\boldsymbol{P}}_f+\boldsymbol{C}_{ff}\boldsymbol{P}_f+\boldsymbol{T}_{ff}\boldsymbol{P}_f-\boldsymbol{T}_{fm}\boldsymbol{P}_m-\boldsymbol{F}^{\text{int}}=\boldsymbol{F}^{\text{ext}}.\tag{24}$$

The definition of the coefficient matrices and the flux vectors is given in "Appendix".

The direct solution procedure is used to discretize Eqs. 23 and 24 in the time domain, and the iterative algorithm is implemented to linearize the nonlinear system of equations.

Numerical example

In this section, a case is utilized to determine the reliability of the improved XFEM–DPM model for multi-scale flow in fractured shale gas reservoir. The basic data (Table 1) of the case are from Civan et al. (2011) and Guo et al. (2012).

A horizontal well with two vertical hydraulic fractures in shale is producing gas in a condition of constant wellbore flowing pressure.

Figures 3, 4 and 5 show the pressure contours of the matrix system corresponding to the production time 0.1, 10 and 1000 days, respectively. Figures 6, 7 and 8 show the pressure contours of the fracture system corresponding to the production time 0.1, 10 and 1000 days, respectively.

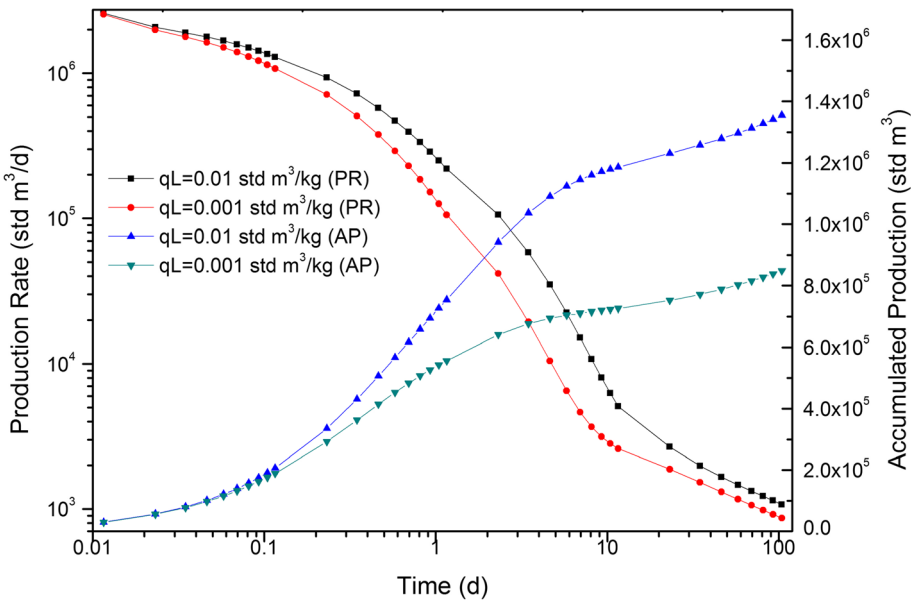

Fig. 9 Impact of the Langmuir gas volume q_L on the production rate (PR) and the accumulated production (AP)

Figures 9, 10 and 11 show the transient production rate and the accumulated production versus time.

As the production time increases, both the matrix pressure and the fracture pressure decrease, but the fracture pressure falls faster.

Figures 3, 4 and 5 indicate that for a long period, the matrix pressure inside the SRV domain decreases faster than that outside the SRV where the matrix pressure hardly decreases. So in the early to middle production period, it can be inferred that the SRV domain determines the main contribution of gas production, and to some extent, the contribution of the matrix domain outside the SRV can even be negligible. After a long period, the matrix pressure drop somewhere outside the SRV domain becomes obvious.

Figures 6, 7 and 8 show a dramatic change in the fracture pressure distribution. Because the micro-mecro scale fracture networks are directly linked to the macroscale fractures and the permeability of the fracture system is higher than that of the matrix, it is reasonable that the pressure of the fracture system falls faster than the matrix pressure for a long time. However, as the porosity of the fracture system is lower, the fall of the fracture pressure slows down.

Figures 9, 10 and 11 separately show the impact of Langmuir gas volume, matrix–fracture transfer shape

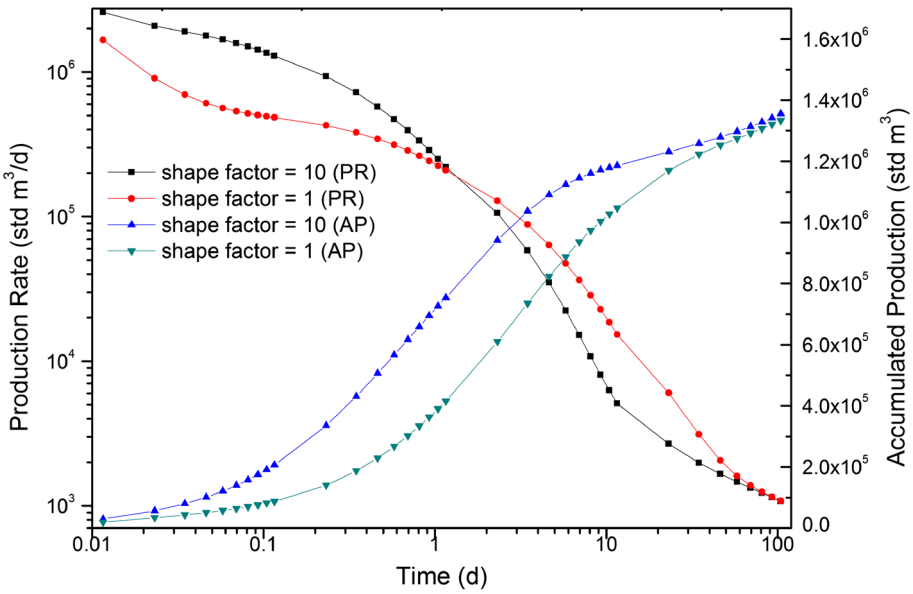

Fig. 10 Impact of the matrix–fracture transfer shape factor on the production rate (PR) and the accumulated production (AP)

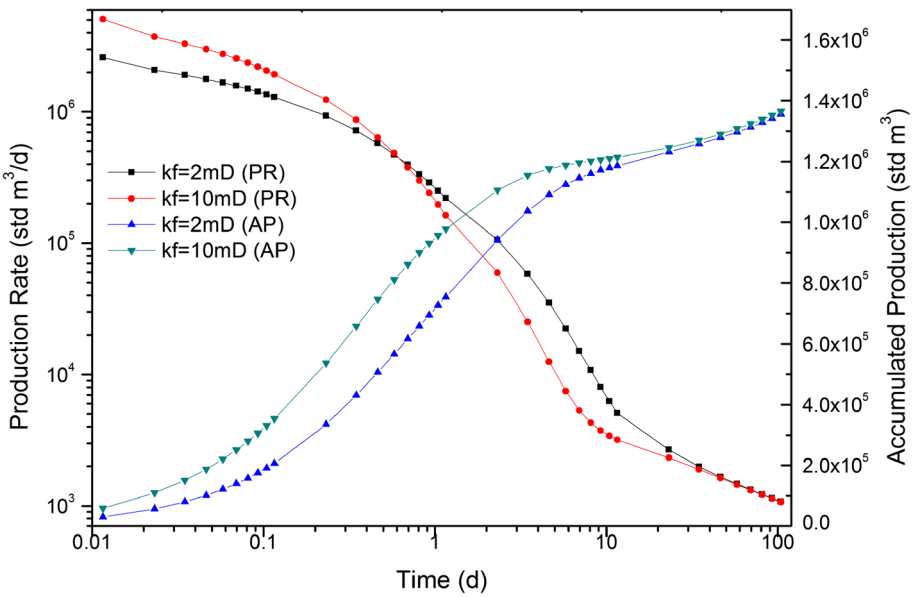

Fig. 11 Impact of the micro-mecro scale fracture permeability on the production rate (PR) and the accumulated production (AP)

factor and micro-mecro scale fracture permeability on production rate and accumulated production.

Figure 9 shows that when Langmuir gas volume increase, both production rate and accumulated production increase. Moreover, the gap of the accumulated productions resulted from the different Langmuir gas volume increases rapidly with time.

Figures 10 and 11 indicate that matrix–fracture transfer shape factor and micro-mecro scale fracture permeability have a similar impact. As the influential factor decreases, the decline curve tends to be gentle. The bigger the influential factor, the higher the initial production. However, for a long time in the later stage, there is an opposite situation. In addition, the different accumulated production curves tend to merge in the final stage, which indicates that the two influential factors do not influence the ultimate shale gas recovery.

Concluding remarks

This paper presents an improved XFEM–DPM model for multi-scale flow in fractured shale gas reservoir and the corresponding solution scheme.

Due to their different effects on shale gas flow, fractures are subsumed under two scales (micro-mecro scale fractures and macroscale hydraulic fractures). The notion of SRV is highlighted to reflect the coverage area (namely inner reservoir) of micro-mecro scale fracture networks and its impact on the drainage of shale gas.

The Lagrangian multiplier method is integrated to introduce the internal well boundary condition so that the physical condition can be asymmetrical.

The case study illustrates the reliability of the improved model and its favorable prospect in engineering application. Sensitivity analyses are conducted to quantify the effects of Langmuir gas volume, matrix–fracture transfer shape factor and micro-mecro scale fracture permeability on production rate and accumulated production.

Acknowledgments The research is supported by the Major Program of the National Natural Science Foundation of China (51490653), Sichuan Provincial Youth Science and Technology Fund (2012JQ0010), Program for New Century Excellent Talents in University (NCET-11-1062), and National Science Fund for Distinguished Young Scholars of China (51125019).

Appendix

The coefficient matrices in the discretized governing Eqs. 23 and 24 are defined as follows:

$$\boldsymbol{Q}_{mm} = \int_{\Omega} \left\{ \begin{array}{l} [N_m \quad N_m^{\text{enr}}]^T \cdot \left[\begin{array}{l} \rho_m \varphi_m C_{tm} - q_L \varphi_m \beta_\phi \\ +(1-\varphi_m) C_a \rho_m \beta_\rho \end{array} \right] \\ \cdot [N_m \quad N_m^{\text{enr}}] \end{array} \right\} d\Omega$$

$$\boldsymbol{Q}_{ff} = \int_{\Omega_s} \left\{ \begin{array}{l} [N_f \quad N_f^{\text{enr}}]^T \cdot (\rho_f \varphi_f C_{tf}) \\ \cdot [N_f \quad N_f^{\text{enr}}] \end{array} \right\} d\Omega$$

$$\boldsymbol{C}_{mm} = \int_{\Omega} \left\{ \begin{array}{l} [B_m \quad B_m^{\text{enr}}]^T \cdot \left(\rho_m \dfrac{K_m}{\mu_m} \right) \\ \cdot [B_m \quad B_m^{\text{enr}}] \end{array} \right\} d\Omega$$

$$\boldsymbol{C}_{ff} = \int_{\Omega_s} \left\{ \begin{array}{l} [B_f \quad B_f^{\text{enr}}]^T \cdot \left(\rho_f \dfrac{K_f}{\mu_f} \right) \\ \cdot [B_f \quad B_f^{\text{enr}}] \end{array} \right\} d\Omega$$

$$\boldsymbol{T}_{mm} = \int_{\Omega_s} \left\{ \begin{array}{l} [N_m \quad N_m^{\text{enr}}]^T \cdot \left(\alpha \dfrac{\rho_m K_m}{\mu_m} \right) \\ \cdot [N_m \quad N_m^{\text{enr}}] \end{array} \right\} d\Omega$$

$$\boldsymbol{T}_{mf} = \int_{\Omega_s} \left\{ \begin{array}{l} [N_m \quad N_m^{\text{enr}}]^T \cdot \left(\alpha \dfrac{\rho_m K_m}{\mu_m} \right) \\ \cdot [N_f \quad N_f^{\text{enr}}] \end{array} \right\} d\Omega$$

$$\boldsymbol{T}_{fm} = \int_{\Omega_s} \left\{ \begin{array}{l} [N_f \quad N_f^{enr}]^T \cdot \left(\alpha \dfrac{\rho_m K_m}{\mu_m} \right) \\ \cdot [N_m \quad N_m^{enr}] \end{array} \right\} d\Omega$$

$$\boldsymbol{T}_{ff} = \int_{\Omega_s} \left\{ \begin{array}{l} [N_f \quad N_f^{\text{enr}}]^T \cdot \left(\alpha \dfrac{\rho_m K_m}{\mu_m} \right) \\ \cdot [N_f \quad N_f^{\text{enr}}] \end{array} \right\} d\Omega$$

$$\boldsymbol{F}^{\text{int}} = -\int_{\Gamma_d} \left\{ \begin{array}{l} [N_f \quad N_f^{\text{enr}}]^T \cdot (w_d \rho_F \varphi_F C_{tF}) \\ \cdot [N_f \quad N_f^{\text{enr}}] \dot{\boldsymbol{P}}_f \end{array} \right\} d\Gamma - \int_{\Gamma_d} \left\{ \begin{array}{l} [B_{fx'} \quad B_{fx'}^{\text{enr}}]^T \cdot \left[\dfrac{w_d \rho_F k_{x'F}}{\mu_F} R(r) \right] \\ \cdot [B_{fx'} \quad B_{fx'}^{\text{enr}}] \boldsymbol{P}_f \end{array} \right\} d\Gamma$$

$$\boldsymbol{F}^{\text{ext}} = \int_{\Gamma_w} [N_f \quad N_f^{\text{enr}}]^T R(r) \cdot \bar{q}_w d\Gamma - \int_{\Gamma_\phi} \left[\frac{\rho_F k_{x'F}}{\mu_F} R(r) \right] \left(\begin{array}{l} [N_f \quad N_f^{\text{enr}}]^T [B_{fx'} \quad B_{fx'}^{\text{enr}}] \boldsymbol{P}_f \\ + [B_{fx'} \quad B_{fx'}^{\text{enr}}]^T [N_f \quad N_f^{\text{enr}}] \boldsymbol{P}_f \end{array} \right) d\Gamma + \int_{\Gamma_\phi} [B_{fx'} \quad B_{fx'}^{\text{enr}}]^T \left[\frac{\rho_F k_{x'F}}{\mu_F} R(r) \right] p_{wf} d\Gamma$$

The existence of the enrichment terms in the above matrices depends on the support domain of the enriched nodes.

References

Belytschko T, Black T (1999) Elastic crack growth in finite elements with minimal remeshing. Int J Numer Methods Eng 45(5): 601–620

Brown M, Ozkan E, Raghavan R, Kazemi H (2011) Practical solutions for pressure-transient responses of fractured horizontal wells in unconventional shale reservoirs. Eval Eng 14(06): 663–676

Carratú JC (2013) Sensitivity of Fractured Horizontal Well Productivity to Reservoir Properties in Shale-gas Plays. PhD thesis, Colorado School of Mines

Cheng WX (1999) Finite element method. Tsinghua University Press, China

Cherubini Y, Cacace M, Blocher G et al (2013) Impact of single inclined faults on the fluid flow and heat transport: results from 3-D finite element simulations. Environ Earth Sci 70(8): 3603–3618

Cipolla CL, Lolon EP, Erdle JC, Rubin B (2010) Reservoir modeling in shale-gas reservoirs. Eval Eng 13(04):638–653

Civan F, Rai CS, Sondergeld CH (2011) Shale-gas permeability and diffusivity inferred by improved formulation of relevant retention and transport mechanisms. Transp Porous Media 86(3):925–944

Dershowitz B, LaPointe P, Eiben T, Wei L (2000) Integration of discrete feature network methods with conventional simulator approaches. Eval Eng 3(02):165–170

Furui K, Zhu D, Hill AD (2003) A rigorous formation damage skin factor and reservoir inflow model for a horizontal well. Prod Facil 18(03):151–157

Guo B, Yu X, Khoshgahdam M (2009) A simple analytical model for predicting productivity of multifractured horizontal wells. Eval Eng 12(06):879–885

Guo J, Zhang L, Wang H, Feng G (2012) Pressure transient analysis for multi-stage fractured horizontal wells in shale gas reservoirs. Transp Porous Media 93(3):635–653

Huang Y, Zhou ZF, Wang JG et al (2014) Simulation of groundwater flow in fractured rocks using a coupled model based on the method of domain decomposition. Environ Earth Sci 72(8):2765–2777

Kristinof R, Ranjith PG, Choi SK (2010) Finite element simulation of fluid flow in fractured rock media. Environ Earth Sci 60(4):765–773

Lamb A, Gorman G, Gosselin O, Onaisi A (2010) Coupled deformation and fluid flow in fractured porous media using dual permeability and explicitly defined fracture geometry. In: 72nd EAGE conference and exhibition

Lee SH, Jensen CL, Lough MF (2000) Efficient finite-difference model for flow in a reservoir with multiple length-scale fractures. SPE J 5(03):268–275

Lemonnier P, Bourbiaux B (2010) Simulation of Naturally Fractured Reservoirs. State of the Art Part 2 Matrix-Fracture Transfers and Typical Features of Numerical Studies. Oil Gas Sci Technol Rev.IFP. Institut Français du Pétrole 65(2):263–286

Medeiros F Jr (2007a) Semi-analytical pressure-transient model for complex well- reservoir systems. PhD thesis, Colorado School of Mines

Medeiros F, Kurtoglu B, Ozkan E, Kazemi H (2007b) Analysis of production data from hydraulically fractured horizontal wells in tight heterogeneous formations. Society of Petroleum Engineers

Melenk JM, Babuška I (1996) The partition of unity finite element method: basic theory and applications. Comp Methods Appl Mech Eng 139(1):289–314

Moës N, John Dolbow, Belytschko T (1999) A finite element method for crack growth without remeshing. Int J Numer Methods Eng 46(1):131–150

Moës N, Cloirec M, Cartraud P, Remacle J-F (2003) A computational approach to handle complex microstructure geometries. Comp Methods Appl Mech Eng 192:3163–3177

Mohammadnejad T, Khoei AR (2013a) An extended finite element method for hydraulic fracture propagation in deformable porous media with the cohesive crack model. Finite Elem Anal Des 73:77–95

Mohammadnejad T, Khoei AR (2013b) Hydro-mechanical modeling of cohesive crack propagation in multiphase porous media using the extended finite element method. Int J Numer Anal Methods Geomech 37(10):1247–1279

Ozkan E, Brown ML, Raghavan R, Kazemi H (2011) Comparison of fractured-horizontal- well performance in tight sand and shale reservoirs. Eval Eng 14(02):248–259

Réthoré J, Borst RD, Abellan MA (2007) A two-scale approach for fluid flow in fractured porous media. Int J Numer Methods Eng 71(7):780–800

Réthoré J, Borst RD, Abellan MA (2008) A two-scale model for fluid flow in an unsaturated porous medium with cohesive cracks. Comp Mech 42(2):227–238

Sheng M, Li G, Shah SN, Jin X (2012) Extended Finite Element Modeling of Multi-scale Flow in Fractured Shale Gas Reservoirs. Society of Petroleum Engineers

Sukumar N, Chopp DL, Moës N, Belytschko T (2001) Modeling holes and inclusions by level sets in the extended finite-element method. Comp Methods Appl Mech Eng 190(46):6183–6200

Warren JE, Root PJ (1963) The behavior of naturally fractured reservoirs. SPE Journal